2000

Holographic Optical Tweezers: Development and Analysis of the First Holodeck Prototype

Matthew T. Dearing '00
Illinois Wesleyan University

Holographic Optical Tweezers: Development and Analysis of the First Holodeck Prototype

by

Matthew T. Dearing

April 2000

Laboratory for Mesoscopics and Quantum Microscopies

Department of Physics

Illinois Wesleyan University
Bloomington, Illinois 61702-2900

Table of Contents

Abstract

Tightly focused light can be used to non-invasively trap and manipulate micro-objects, a technique called "optical tweezing." By utilizing the large field gradients present in a focused laser beam, micro-particles—including biological specimens and many other materials—can become confined in all three dimensions. While optical tweezing has existed for over a decade, it has generally been limited to trapping one or two particles at a time. We have developed a technique that uses laser light to assemble large numbers of micro-particles in a highly controllable way. Here we describe, for the first time, the *complete* implementation of holographic optical tweezer arrays ("HOT" arrays), which offer a new means of simultaneously directing the assembly of particles into any configuration.

Through calculation, and subsequent fabrication of, holographic optical devices, we can sculpt a single laser beam into a fully-configurable array of optical tweezers. Each spot in such an array is then capable of trapping and manipulating one particle, making possible *simultaneous* control over large collections of micro-objects. Our addition of holographic techniques has extended the basic capabilities of optical tweezing, making it a more viable tool for the assembly of nanodevices and the organization of specimens into user-defined structures.

Previously, a generalized Lorentz-Mie scattering theory has been used to model *single* (non-holographic) optical traps. Here, we develop a simpler and more intuitive approach to examine the trapping potential as a function of particle size, the polarizability of the particle material as compared to that of the surrounding medium, the power of the laser used to trap the particles, and the angular divergence of the optics used for

promoting assembly. For this calculation we incorporate an approximate form for the energy density of the laser beam—one that is appropriate both within and outside of the Rayleigh limit. We believe that our conclusions remain viable in the intermediate case, where the particles to be trapped have dimensions on the order of the wavelength of visible light; this regime is of particular interest in applications involving assembly of photonic bandgap materials and other photonically-active structures. Notably, we are the first to address the key question regarding application of holographic optical tweezer arrays, namely the *number* of particles that can be simultaneously incorporated and manipulated.

There are many potential applications for such techniques; *e.g.*, allowing for the construction of aggregations with tailor-made crystalline symmetries. Defects may be introduced in a controlled way allowing exploration of their role in phase transitions. Even biological specimens could be organized into useful configurations for studying how they behave in large, organized collections. In addition, there is growing interest in electronic devices, which exploit the confinement of electrons onto *isolated* nanoparticles. The application of our techniques might increase the yield during fabrication of these devices.

List of Figures and Tables

I. Introduction

A single optical tweezer can be formed by tightly focusing a laser beam with a microscope objective lens,[1] or by using the evanescent or near-evanescent fields produced by illuminating a sub-wavelength aperture under certain conditions.[2] The resulting optical gradient forces can non-invasively manipulate a dielectric microparticle,[3-5] a biological specimen[6-10] and even metallic nanoparticles[11] and neutral atoms[12]

Although optical tweezers have been a valuable research tool since their development[3] in the 1980s, they have remained limited to trapping only one particle per laser beam. Previously, beam splitters have been used to create multiple traps,[13-14] and such a scheme has been used to position two particles for interaction measurements.[15-16] Cylindrical lenses or line scanning can be utilized to form elongated tweezers,[17] which can trap several micro-particles into 1-D arrays. Up to now, optical tweezers were unable to assemble micro-particles into *any* configuration since increasing the number of lasers or discrete beam splitting elements is cumbersome, and unreasonable for large, multidimensional arrays.

A commercially-available transmission hologram was recently incorporated into an optical tweezer setup,[18] providing a simple means of assembling sixteen particles. To move beyond this first prototype, we have produced computer-generated holograms, which, when used in optical tweezing, can produce functional structures or arrays of traps with tailored symmetries and/or defects—all on scientifically interesting length scales (*e.g.*, those where interactions between trapped particles become relevant).

We can digitize any image and convert it to a "calculated hologram" via an algorithm of iterative approximation. We then fabricate our own "designer hologram," which is a physical manifestation of this calculation. In our optical apparatus, the hologram sculpts the focused laser light into a user-defined optical potential composed of many tailored optical tweezers, each capable of trapping one micro-particle.

Our holographic optical tweezers can assemble *large numbers* of micro-particles in a *highly controllable* way. However, the desire to extend this technique towards the inclusion of *very* large numbers of particles comes at a cost: the available laser radiation is now to be divided among many separate traps.

By incorporating holographically generated arrays of optical traps we can fabricate controlled assemblies, and perhaps devices, out of nanometer-scale components. For example, future work may exploit holographic optical tweezers to aid in the fabrication of photonic bandgap materials[19-21] and optical circuit elements.[18] Also, self-assembled nanoelectronics created from colloidal arrangements might prove to be an important technological advancement as computer chips become more compact.

In addition to new device fabrication, further applications are envisioned in many different disciplines including biology, chemistry, and condensed matter physics. For example, interactions between colloidal particles have previously been studied by using one or two laser beams to trap one or two particles.[22] Our interest is studying the many-body limit. Initially, our work is focusing upon large *ordered* arrangements of charge-stabilized colloidal suspensions, providing a model system for studying the microscopic mechanisms of structural phase transitions.[23-32] Using colloidal systems as models is advantageous because the interacting particles are large enough to be imaged in real time

with an optical microscope, yet they are also small enough that thermal energy is important. Thus, the equilibrium thermodynamics of the system can be studied.

In this paper, we successfully demonstrate, for the first time, the *complete* implementation of holographic optical tweezers. We first describe the key considerations at each stage of fabrication and implementation and we show that although such optically assembled structures are limited by the available laser power and several other factors, this technology is currently viable and capable of immediate application.

II. The Physics of Optical Tweezers

There are two necessary conditions that must be provided if an optical tweezer is to successfully trap a small particle. First, depending on the particle's environment, the potential well formed by the concentrated electromagnetic field must be deep enough to hold the particle against external energies; for example, the buffeting of Brownian motion if the particle is in solution. Second, the trapping force due to the intensity gradient must be large enough to direct the particle to the trap location (*i.e.*, the focus) and act as a restoring force keeping the particle in the trap.

The explanation for the physical origin of these trapping conditions in an optical tweezer depends upon which of several physical limits is involved. Dielectric particles much larger than the laser wavelength ($R >> \lambda$) will essentially act like a converging lens for the incident light, so a simple geometrical, or ray optics approach may be applied to determine the trapping force vectors. This method vector-sums the momentum of all contributing light rays, where the resultant represents a change in momentum (*i.e.*, the axial trapping force).[4] One important prediction of this model is that the exerted force on the particle becomes independent of particle size. In the opposite limit, called the Rayleigh regime where the particle is much smaller than the laser wavelength ($R << \lambda$), aseparate approach must be taken by solving Maxwell's electromagnetic equations,[5] since the dielectric particle can be approximated as a simple point dipole in an electric field. For our purposes here, where we derive a more intuitive expression for the potential (which includes a smooth transition from the Rayleigh to ray optics limits), it will suffice to provide a *simplified* description of the physical origins of optical trapping.

The particles used in these experiments are either polystyrene sulfate or silica spheres, although any particle may be trapped as long as it is a *dielectric* and, therefore, will be polarized (*i.e.*, the charges within the particle will separate) by an applied electric field, $\boldsymbol{E}_A$. When the charges redistribute, a small electric field, $\boldsymbol{E'}$, results and opposes the applied $\boldsymbol{E}_A$ (*i.e.*, the laser's electric field). The overall, or effective, electric field, $\boldsymbol{E}_{eff}$, of the system diminishes (Fig. 1).

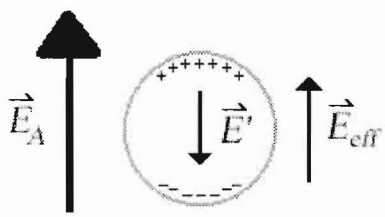

Figure 1. A schematic drawing of a dielectric particle in an applied electric field, $\boldsymbol{E}_A$. $\boldsymbol{E'}$ is the induced field due to the redistribution of charges within the particle and $\boldsymbol{E}_{eff}$ is the resulting effective electric field, which is the vector sum of $\boldsymbol{E}_A$ and $\boldsymbol{E'}$. As the induced field within the dielectric will be opposite to that of the applied field, the effective field will always be smaller and correspond to a smaller energy of the system.

There is an energy cost associated with the presence of an electromagnetic field. When the particle polarizes within the laser beam and the resulting $\boldsymbol{E}_{eff}$ is less than $\boldsymbol{E}_A$, then less energy is required of the entire system (composed of the particle and the laser beam). At the focal point, the applied field has its largest magnitude (the intensity), so if the dielectric particle is located at this point, the polarization is largest and the least energy of the system is obtained.

A. Optical Tweezer Potential

In order to quantify the potential well formed by the concentrated electromagnetic wave, we present an intuitive, approximate calculation of the potential well depth due to the gradient force as a function of particle size. This calculation is reasonable over a wide range of particle sizes, but it does not take into account all of the complicating factors present in a HOT system; a later section discusses new features that can arise in HOT arrays.

1. Gaussian Beams

Although holographic optical tweezers can generate line traps and many other sorts of tailored potentials, for the purposes of this calculation we consider a transmission hologram that generates an array of laser spots. If the beam incident upon the hologram has a Gaussian profile, then in the far-field limit each of our output beams will also be Gaussian. In our system, each of these output beams is to be focused with a microscope objective lens to a diffraction-limited spot where trapping occurs. So, to describe the profile of an individual output beam as it approaches its focus, we define a radius, ω, referred to as the beam waist. In our definition, we take ω to be the standard deviation, σ, of the Gaussian intensity profile of the output beam under consideration. This is not a universal convention for describing Gaussian optics; many others[33] use $\omega = 2\sigma$. However, it will turn out that the maximal restoring force on a small particle ($R << \omega$) occurs when it has moved from a transverse distance equal to our beam waist; this is the point of inflection of the Gaussian, and therefore the point where the trapping potential has its maximal slope and the optical gradient forces are largest.

We use a hyperboloid function to describe the beam waist as a function of axial position, z. This simple form provides appropriate limiting behaviors both near and far away from the focal point:

$$\omega = \sqrt{\omega_0^2 + z^2 \tan^2(\nu)} \tag{1}$$

Here ν represents the divergence from the z-axis as the empty beam moves away from the focal point and ω_0 characterizes the size of the diffraction-limited spot.

We estimate the minimum beam waist to be $\omega_0 = 1.22(f\lambda)/(2a)$, where a is a diameter describing vignetting in the optical path. (Note that the factor of two in the denominator comes from our definition of the beam waist.) Our laser wavelength, λ_0, is 532 nm, which should be corrected for the medium of propagation (in our work, water) to be: $\lambda = (532\text{ nm})/n_0$. If tweezing occurs via an objective lens for which the focal length and diameter of the back aperture are $f = 1.62$ mm and $a = 3.24$ mm, respectively, we estimate $\omega_0 = 124$ nm.

The angular divergence of light focused by an oil-immersion lens is written, in most texts, as $\nu' = \arcsin(N.A./n_{\text{oil}})$. However, given our unconventional definition of the beam waist, we use an angular divergence, ν, such that $\tan(\nu') = 2\tan(\nu)$. Since our objective lens has a numerical aperture of 1.4 and is used with oil having the same index of refraction as the cover slip ($n_{oil} = 1.515$, which is also quite close to the index of refraction of the colloidal silica particles used in our experiments), $\nu' = 67.53°$, and $\nu = 50.4°$. Note that when we trap an array of particles from a colloidal suspension of

silica spheres in water, the tail of the incident distribution suffers total internal reflection. This should not introduce any errors in the small particle limit, and even for larger particles the percentage of intensity lost in this way is not significant. If necessary, additional optics may be used to adjust the beam width as it enters the back aperture of the objective lens, thereby limiting the amount of light lost in this manner.

2. Energy Density

Given our hyperboloid waist function, conservation of energy implies that the intensity of a Gaussian beam can be written in cylindrical coordinates as:

$$Intensity(\rho,z)=\frac{Pe^{-\frac{\rho^2}{2\omega(z)^2}}}{2\pi\omega(z)^2} \tag{2}$$

where the laser power is $P=\int Intensity\, dA$. To find the energy density, η, inside the particle we simply divide the intensity by the speed of light in that medium:

$$\eta(\rho,z)=\frac{Intensity(\rho,z)}{c/n} \tag{3}$$

This amounts to a paraxial approximation to the fields, but the errors introduced are not likely to be more than 10% even in our most extreme case.[34] We plot, in Fig. 2, η as a function of the radial coordinate (at $z = 0$, the focal point), both to highlight the Gaussian nature of the form provided and to emphasize our definition of ω.

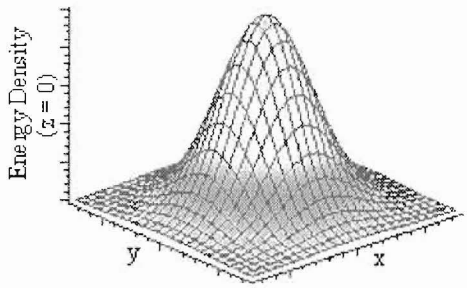

Figure 2: A slice of the energy density, η, at the focal point ($z = 0$) as a function of the radial coordinate, ρ. Note that the graph has been converted to Cartesian coordinates. For our purposes, the beam waist, ω_0, is defined as the radius at the point of inflection on the Gaussian energy density distribution.

3. Reduction of Electromagnetic Energy

As described above in our simplified explanation of the effective electric field, the energy *reduction*, U, which occurs when a dielectric particle sits at the focal point, (as opposed to a point far outside of the laser beam), is determined by the local energy density and the relative polarizability[35] of the particle to be trapped, $\alpha = \varepsilon/\varepsilon_0 - 1$. For silica particles in water, α compares the dielectric constant of silica, $\varepsilon = 2.3$, to that of water, $\varepsilon_0 = 1.7$. The reduction in electromagnetic energy can be found by integrating the product of the relative polarizability and the energy density over the volume of the particle:

$$U(R) = \alpha \int_0^R \int_{-\sqrt{R^2-\rho^2}}^{\sqrt{R^2-\rho^2}} \int_0^{2\pi} \eta(\rho, z)\rho d\varphi dz d\rho \qquad (4)$$

For our optics, a 1 mW beam incident upon a 1 μm silica particle (0.5 μm radius) immersed in water yields $U = 6.3$ eV as the amount of energy saved when the particle sits at the center of the trap.

We can compare the results of our simple model to those derived from a more extensive treatment thought to be valid in the Rayleigh limit. Harada and Asakura[5] find the depth of the trapping potential to be

$$U_{Harada}(R) = 2\pi R^3 \frac{\sqrt{\varepsilon_0}}{c}\left(\frac{\varepsilon - \varepsilon_0}{\varepsilon + 2\varepsilon_0}\right)\frac{2P}{\pi(2\omega_0)^2} \tag{5}$$

Again, this is the potential associated with the gradient force alone, for a *small* particle ($R << \omega_0$) at the focal point. This model yields a potential well depth of 0.2 meV for a 10 nm particle, which differs from our simpler model (for the same particle size) only by a factor of two. It should be noted that we have modified the formula of Harada and Asakura to be in keeping with our definition of the beam waist, so the small difference mentioned above is genuine; however, as the particle size increases, Harada and Asakura's R^3 dependence overestimates the trapping strength. On the other hand, *our* model provides a clear physical explanation of the small-particle R^3 dependence and includes the expected roll-off as particle size grows beyond the Rayleigh limit.

The log-log plot shown in Fig. 3 clearly indicates that for particles which are smaller than the minimum beam waist, our calculated U goes as R^3, since the reduction in electromagnetic energy merely scales with the volume of the trapped particle. As the particle size is increased beyond this range, the deviation from this R^3 dependence

becomes clear. For particles much larger than the minimum beam waist, U is proportional to R. In the intermediate region, no simple dependence emerges.

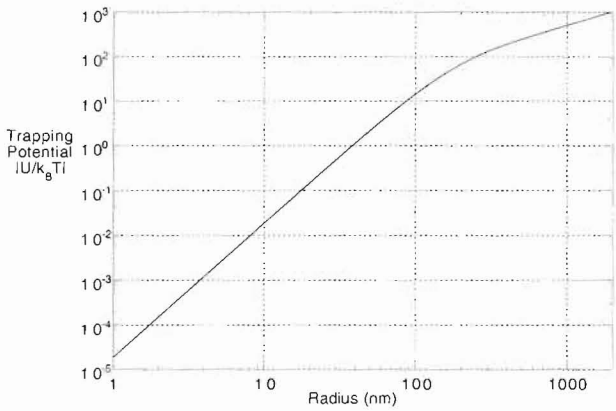

Figure 3: The depth of the trapping potential, U, as a function of particle radius, R, given the system parameters outlined in the text. The R^3 dependence begins to change between 100 and 200 nm, which is around our minimum spot size, ω_0 = 124 nm. By $R \sim 2\omega_0$ the large-particle dependence is established.

Still, it is clear that in our model the depth of the potential well created by optical tweezing monotonically increases as the amount of material contained within the laser field increases. After all, increasing R merely increases the limits on the integration in Eq. 4 and given the Gaussian nature of the integrand this can only increase the magnitude of the result. That is, within this model the electromagnetic energy of the system *must always* be reduced by having more of the region of non-zero field taken up by a particle that is more polarizable than the surrounding medium. It might now seem that a larger particle always results in a better, or stronger, trap. However, there are additional factors that will be considered later, some of which are generic to optical tweezing, some of which are unique to HOT arrays and some of which are particular to trapping from colloid (and would not be found when, say, trapping in vacuum).

B. Optical Tweezer Forces

As previously mentioned, there are several limits in which the forces involved in an optical tweezer can be described. For particles much larger than the wavelength of the laser beam, a spherical particle will act similar to a converging lens. As the rays are further focused by the dielectric particle, a change in momentum occurs resulting in a force on the particle directed toward the center of the focused laser spot. However, in this paper we will approximate the forces only in the Rayleigh limit where the particle size is much smaller than the wavelength. Although this formulation is not valid for larger particles, it does provide another clear picture for the physical origins of the forces.

As a laser passes through the objective lens (typically, 100×, 1.4 N.A.) of a microscope, it is focused to a diffraction limited spot of diameter, ω_0. Passed this focal point along the optical path, the electric field's intensity is changing as the laser is unfocusing; the beam spreads out and becomes less concentrated. This changing intensity, or an intensity gradient, results in a force directed toward the laser focus, which is the direction of maximum change (as is defined by a gradient). A particle entering this gradient field will feel a force that causes it to move toward the focal point. The gradient force is present from both directions along the optical axis and tends to keep the particle within the focused spot (Fig. 4a).

a. b.

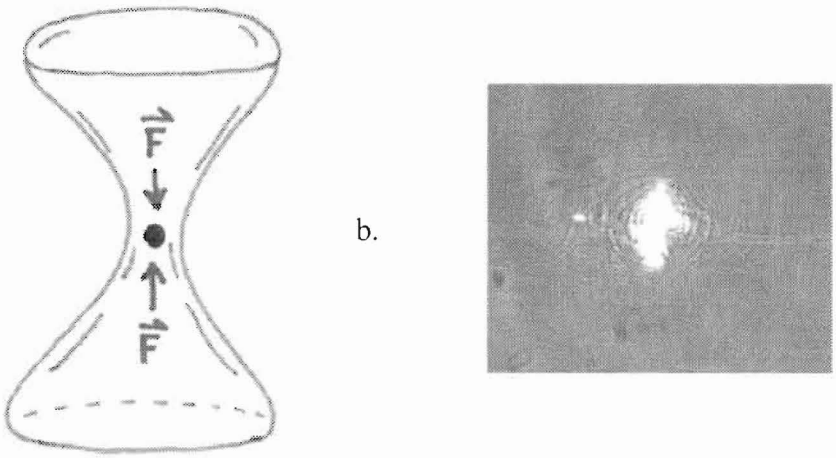

Figure 4: (a) In this schematic profile of an optical trap, the laser beam is being focused to a tight spot of radius ω_0 by a microscope objective lens (not shown). Gradient forces resulting from the changing intensity of the beam point towards the focus and traps a particle in three-dimensions. (b) An actual optical tweezer spot imaged from above.

As expressed in Ref. 5, the gradient force on a particle with dielectric constant ε and a surrounding medium with dielectric constant ε_0 placed in a optical field with Poynting vector **S**,

$$\vec{F}_{\nabla} = 2\pi R^3 \frac{\sqrt{\varepsilon_0}}{c}\left(\frac{\varepsilon - \varepsilon_0}{\varepsilon + 2\varepsilon_0}\right)\nabla\left|\vec{S}\right| \qquad (6)$$

The Poynting vector, **S**, describes the flow of energy, and its absolute value is the intensity of the electromagnetic wave.[36] As described above, it can be seen that Eq. 6 tends to bring the particle toward the region of highest intensity (*i.e.*, the focus).

However, a competing force is present in an optical tweezer system caused by momentum transfer from the photons of the electromagnetic field to the particle. This

radiation pressure, commonly referred to as a scattering force, is directed opposite the focus and tends to cause the particle to move slightly out of focus:[5]

$$\vec{F}_S = \frac{8}{3}\pi(kR)^4 R^2 \frac{\sqrt{\varepsilon_0}}{c}\left(\frac{\varepsilon - \varepsilon_0}{\varepsilon + 2\varepsilon_0}\right)^2 \vec{S} \tag{7}$$

where $k = 2\pi/\lambda$ is the wavenumber of the trapping radiation.

Since both of these forces significantly contribute to the trapping strength of an optical tweezer, we must consider that in the presence of monochromatic light of wavenumber k a dielectric sphere of radius R will experience a total optical force, which is the vector sum of the gradient and scattering forces:

$$\vec{F} = \vec{F} + \vec{F}_S \tag{8}$$

If the scattering force vector is too large, the particle will not be trapped. Thus, we have the second necessary condition for trapping where $\vec{F} / \vec{F}_S > 1$. Fortunately, because $\vec{F}$ is proportional to R^3 while $\vec{F}_S$ depends upon R^6, the scattering force becomes less of a problem for smaller particles. For the purposes of analysis in this paper, we will continue to assume the scattering component is much less than the gradient force, so we can safely ignore its effects for now.

III. Incorporating Transmission (Phase-modulating) Holograms

Diffractive optical elements (DOE) can be incorporated into refractive optic setups in order to make more compact dispersion corrected designs. DOEs can also replace refractive optics that are too difficult to make by grinding or polishing. Phase-modulating DOEs, or transmission holograms, may be used to convert a single laser beam into any user-defined pattern. If focused to a tight spot, the resulting patterned beams are each capable of trapping a micro-particle. Based on this idea, our holographic optical tweezer design allows for the simultaneous trapping and assembly of many particles into arbitrary configurations. As mentioned above, a commercial hologram was previously used to demonstrate this principle,[18] but here we describe the successful implementation of the complete process, from calculation to trap.

A. The Physics of Holograms

Commercially available diffractive optics can alter a *single* laser beam into some pattern of laser spots. We are limited, though, to the diffraction patterns the manufacturers find financially viable. In order to fabricate scientifically interesting and technologically useful structures, we would like to have an increased degree of control where we first state what diffraction pattern we want (some arbitrary pattern, say, a 100 × 100 array of points), then determine what the diffractive optic needs to be to form this pattern and finally, to fabricate the required diffractive optic.

DOEs diffract light from some configuration of opaque and/or transparent regions. The most common diffractive optic is a grating of uniformly spaced slits each with a width comparable to the wavelength of incident light. The grating produces a one

dimensional diffraction pattern composed of a series of light bands with decreasing width and intensity further from the center of the pattern.

This type of grating is an example of and *intensity*-modulated diffractive optic and will necessarily absorb some intensity in its opaque regions. However, as seen in the above examination of the optical potential, the intensity is critical for strong trapping. Therefore, we restrict ourselves to using a particular class of DOEs that only modulates the phase of the input beam so as to minimize the amount of amplitude lost before forming the traps. A *phase*-modulating, or transmission hologram transforms only the phase of an incident wavefront into another output phase.

In other words, the transmission hologram is a *phase mask* for the incident laser light. The spatial phase of a wavefront is the "offset" of the wave from its initialization. If the phase of a sine wave is "$\pi/2$," then the wave begins traveling at its first crest, rather than at zero. Two adjacent waves with their traveling fronts that are in sync with each other are considered to be "in phase." Since we use a coherent laser as our source, the phases of all the wavefronts are the same at the incident boundary of the hologram.

When the wavefront enters the hologram material (say, sapphire or fused silica), the effective speed of the waves slows depending on the material's index of refraction. If all of the waves travel the same distance at the slower speed, then the output waves would still be in phase. However, if on the surface of the hologram we pattern varying depths, the phase of one wavefront relative to a neighboring wavefront will shift if they pass through different material thickness. For instance, if this depth is the same as the length of the wave from its zero position to $\pi/2$, the exiting wave correspondingly has a phase of $\pi/2$. The wavefront is now in a different phase relative to its neighbors and will

either constructively or deconstructively interfere with them based on their phase difference. Since we can program the surface relief in the hologram (see below), this diffraction will produce a programmed pattern of bright and dark spots (Fig. 5).

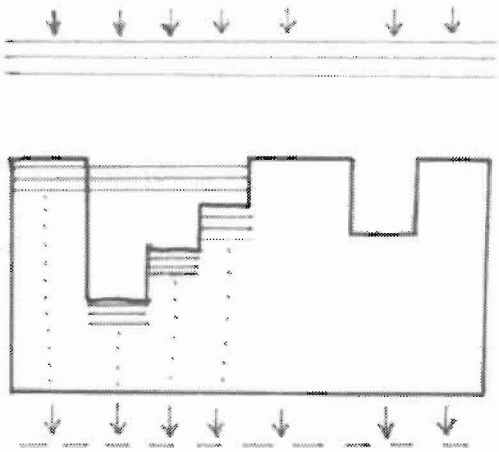

Figure 5: A schematic of a transmission hologram sculpting the input phase of the incident laser radiation. The depths etched into the hologram determine how far a wavefront will travel at a slowed, effective speed emerging with an altered phase relative to a neighboring wavefront. Exiting waves with different phases will produce an interference pattern based on the overall surface relief in the hologram.

B. Calculating the Hologram

Computer-generated holograms enable the creation of very sophisticated optics and provide no limits as to what the final diffraction pattern may look like. Our hologram patterns are calculated using an Iterative Fourier Transform Algorithm (IFTA)[37]. In other words, a random "guess" as to what the pattern should look like can be made, then optimized it until the desired result is obtained.

The electric field of the laser focused in the microscope's field of view is the Fourier Transform of the electric field at the hologram:[37]

$$I_0(u,v) \equiv |F(u,v)|^2 = \left| \int_{-\infty}^{\infty} \int_{-\infty}^{\infty} B_0(x,y) e^{i\Psi(x,y)} e^{\frac{ik}{2z}\left[(x-u)^2+(v-v)^2\right]} dxdy \right|^2 \quad (9)$$

where (x,y) and (u,v) are the coordinates at the hologram and the field of view, respectively, B_0 and Ψ are the amplitude and phase of the input beam, respectively and F and I are the field and intensity at the field of view, respectively.

The intensity in the pattern is extremely important since it is a key factor in causing particles to be trapped. As noted above, we do not want to waste any of the intensity as it passes through the hologram, so we chose to vary only the *phase* of the field and not the amplitude. By controlling the phase of the field at the hologram, we can produce any intensity pattern in the field of view.

Once the intensity pattern is determined, the phase mask is calculated using the Adaptive-Additive Algorithm (based on Gerchberg-Saxon Iterative Algorithm).[37] First, the amplitude and a random phase in radians is set up for the input beam. A Fourier Transform is taken of the this field returning the field at the field of view, or focal plane. Next, the actual intensity pattern is weighted with the calculated amplitude and an inverse Fourier Transform is computed. This returns the field at the hologram and the entire process is iterated until the calculated field at the focal plane matches with the desired intensity pattern (See Table 1). Using this algorithm to control the phase in the input plane, we can control the location of amplitude in the focal plane. The results of this sort of calculation can be seen in Fig. 6a and b, where a digital pattern is iteratively converted to a binary surface relief pattern.

Input

$B_0 = 1$ (amplitude of Gaussian laser beam)	Ψ_0 = random # $0 \rightarrow 2\pi$ (phase of laser)

$W_n = (B_n, \Psi_n)$	$\rightarrow$ (Fourier Transform)	$F_n = \Im\{W_n\} \equiv (A_n, \Phi_n)$
$\uparrow$ (Replace $\overline{B}_n$ with B_0 and $\overline{\Psi}_n$ with Ψ_n)		$\downarrow$ (Add in A_0, the actual pattern desired.)
$\overline{W}_n = \Im^{-1}\{\overline{F}_n\} \equiv (\overline{B}_n, \overline{\Psi}_n)$	$\leftarrow$ (Inverse Fourier Transform)	$\overline{F}_n = (A_0 + \alpha A_n, \Phi_n) \equiv (\overline{A}_n, \overline{\Phi}_n)$

Table 1: A schematic outline of the iterative process used to calculate the hologram pattern from any desired intensity pattern. $W_n = B_n e^{i\Psi_n} \equiv (B_n, \Psi_n)$ represents the wave of the input beam, where B_n and Ψ_n are its amplitude and phase, respectively. $F_n = (A_n, \Phi_n)$ represents the wave at the field of view, where A_n and Φ_n are its amplitude and phase, respectively. A_0 is the actual pattern desired and α is a weighted factor. On all variables, n is the index of the input digital array.

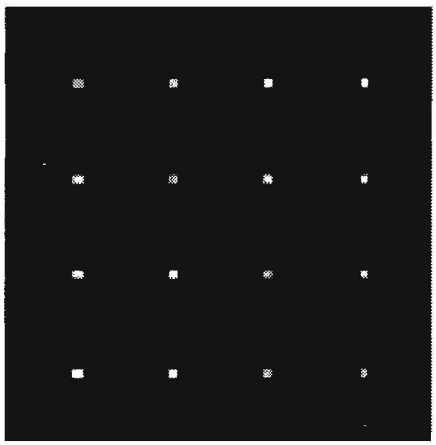

a.

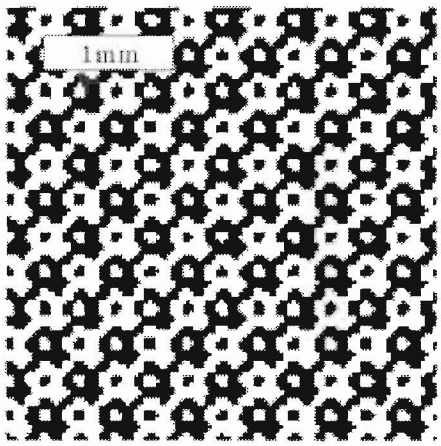

b.

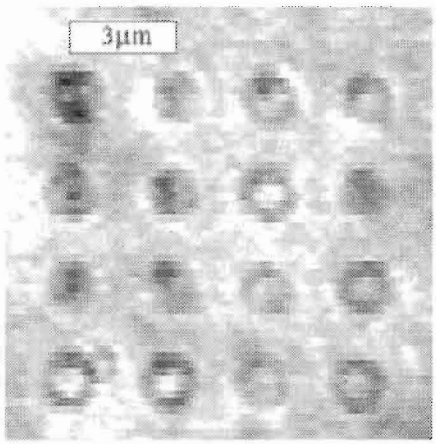

c.

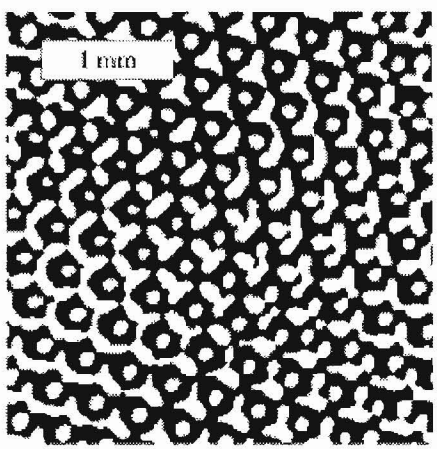

d.

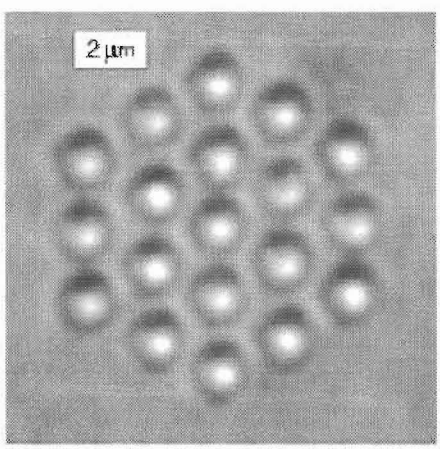

e.

Figure 6: "Designer Holograms." (a) The original input pattern (a digital image) representing a 4 × 4 array of traps. (b) The calculated binary surface relief for a hologram that will produce a 4 x 4 array. (c) A functional HOT array after fabricating the calculated surface relief in (b) into a sapphire substrate. (d) Another hologram surface relief calculated for a hexagonal configuration. (e) The HOT array for the hologram pattern in (d). The patterns were calculated by our collaborator, E. R. Dufresne, at the University of Chicago.

C. Fabricating the Hologram

As a first step, we consider binary holograms (those involving two levels). Fig 6 shows the calculated patterns for a square array and for a hexagonal, close-packed array of spots. In this figure, black pixels are meant to represent an etch depth sufficient to cause a phase shift of 180° relative to light transmitted through unetched regions. In other words, what is shown is the etch mask used in fabricating the hologram.

In order to understand ways to improve hologram efficiency, as well as the sensitivity of the hologram to flaws in the fabrication (*e.g.*, an incorrect etch depth resulting in a phase offset; a lack of uniformity over large distances—flatness; a lack of uniformity over short lengths—roughness), we first examine a far simpler (intensity-modulating) DOE: Young's classic double-slit experiment. If a coherent, monochromatic point source is incident on an opaque screen with two narrow slits separated by a distance, d, then on a screen far away, $d' >> d$, an interference pattern of alternating bright and dark fringes will appear. If the two slits are thin enough, they will act as point sources of two coherent, cylindrical wavefronts. At any point on the imaging screen, the resultant intensity will simply be due to the superposition of the two wavefronts (*i.e.*, the sum of the two wave amplitudes at that point). Since the waves were in phase at the slits, any relative phase difference between the two waves arriving at the imaging screen will be due entirely to the difference in the *path length* they travel. If this path difference is an integral number of wavelengths, then the relative phase shift will be a multiple of 2π, so the waves constructively interfere.

If we compare the two-slit experiment to a similar experiment involving many, equally-spaced slits, we learn an important lesson about the sensitivities of DOE. For an

N-slit diffraction grating, the condition for constructive interference is the same as that for the two-slit experiment: the path difference from adjacent slits to a bright spot on the imaging screen must be an integral multiple of the wavelength. However, there is a key difference: as the number of slits increases, the angular width, $\Delta\theta$, of the interference fringes decreases:[38]

$$\Delta\theta = \frac{2\lambda}{Nd\cos\theta} \tag{10}$$

Crudely, the more information present in the diffracting surface, the more distinct the diffraction pattern can be.

For holographic diffractive optics, we can add more information to the surface in three distinct ways. We could enlarge the area of the hologram; however, there is no advantage to making a hologram with an area larger than that of the illuminating beam. We could reduce the minimum linewidth of features contained in the hologram, thereby packing more information into the same area; however, there is a practical limit on the minimum feature size. Alternatively, more information can be incorporated into the hologram using multiple *layers* as opposed to the simple two-level, or binary, optics we have described so far.

The efficiency of a hologram is measured by looking at how much of the scattered light is contained in the first-order diffraction pattern. Binary optics tend to have efficiencies of 40.5%, whereas holograms with 4, 8, and 16 levels can reach efficiencies of 81%, 95%, and 99%, respectively.[39] Of course, the ideal hologram would have a continuous surface relief. However, the ease and cost-effectiveness of conventional

lithography often leads DOE designers to use discrete-level approximations to these ideal, continuous profiles.

Multilevel hologram fabrication requiring 2^m separate steps, involves a lithography of m iterations of resist spinning, pattern alignment, masking, development, and etching.[40] In other words, the first mask will create a two-level surface relief and each subsequent mask will double the number of phase levels from the previous mask. However, each additional mask must also be accurately registered (*i.e.*, aligned) with previously etched features. Additional errors associated with each iteration (phase offset, flatness, and roughness) are cumulative. Total fabrication errors should be kept below 5-10% of the minimum linewidth and step height for best performance of the resulting hologram.[40]

The transmission holograms we first fabricated utilized standard optical lithography and ion milling techniques. Our mask-making process involved taking a photograph of our computer-generated pattern with (high contrast) Kodak Technical Pan B&W film and then using the developed negative as a mask for conventional photolithography. The grain size of the film limits the resolution of the mask, which was about 3 μm per line pair. For our 4×4 HOT array, each calculated pixel (the smallest possible feature in the pattern) was 12.6 μm wide, so the film's resolution was sufficient to create well-defined opaque regions in the mask. Later, work was done by John Vrakas, another Illinois Wesleyan University student, and myself at the Cornell University National Nanofabrication Facility fabricating glass masks coated with a patterned layer of chrome, which provided a high-quality mask with much greater resolution.

The calculated pattern was then transferred by passing UV light through the mask onto to a substrate (initially sapphire) coated with a polymer (resist layer) that was locally activated by the UV radiation. The resist was then developed, removing the polymer that had been exposed to the radiation. The etched depths needed to provide the required phase shift is found with:

$$depth = \left(\frac{\lambda}{n-1}\right)\left(\frac{phase\ shift}{2\pi}\right) \tag{11}$$

Ion milling was first used to etch all areas of the surface, which were no longer protected by resist. A 500 V, 0.4 mA/cm^2 beam of Ar^+ ions provided an etch rate of about 100 Å per minute for our sapphire substrates (Fig. 7) to a depth of about 3500 Å with an *rms* etched surface variation of about 3.5 Å over 1 μm. For small arrays such as our 4 × 4 HOT, this technique was sufficient to produce efficient holograms that strongly trapped micro-particles (Fig. 6c).

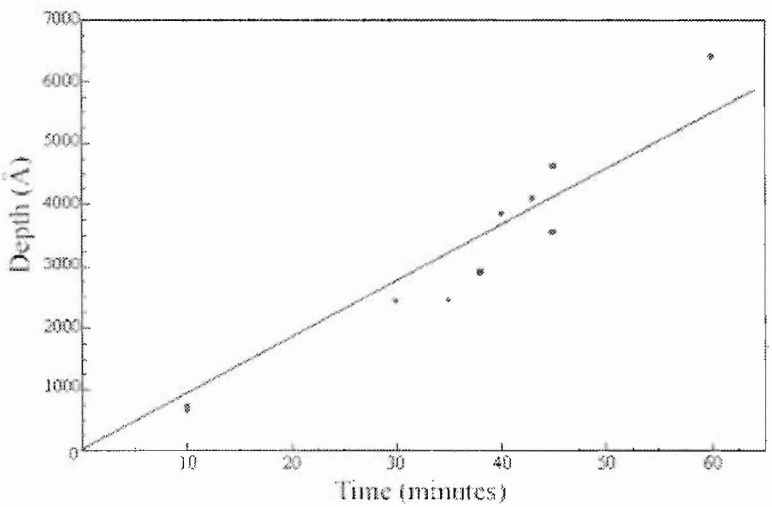

Figure 7: Etching of a sapphire substrate with ion milling resulted in an etch rate of approximately 97 Å per minute. Note: the line is only a guide to the eye.

However, the configuration of optical traps becomes larger and more complicated, the detail required in the hologram becomes finer. As the smallest feature in the hologram approaches the scale of the roughness induced by ion etching, the hologram can no longer function effectively (averaging over roughness cannot occur in these smaller features). One way in which we have attempted to reduce etch-induced roughening is by changing substrate materials from sapphire (which is crystalline and therefore exhibits roughening due to anisotropies inherent in the lattice structure) to fused silica (which is amorphous). Also, since we expect the *rms* roughness to be a function of the energy of the etching process, we moved from ion-milling to Reactive Ion Etching (RIE). So far, RIE has allowed us to achieve better than 0.04 Å *rms* variation of etch depth across 1 μm, however the etch rates are much slower (Fig. 8). This provided an additional complication where the resist layer would be etched away itself before the required substrate depth was attained. To solve this problem, Stephen Sheets, a student at Illinois Wesleyan University, made the resist layer out of chrome, which was capable of sustaining the long RIE. In the future, we intend to produce phase masks without etching, but by spinning on PMDS or PMMA. As we work towards producing smoother patterning, the efficiency of our holograms should continue to improve.

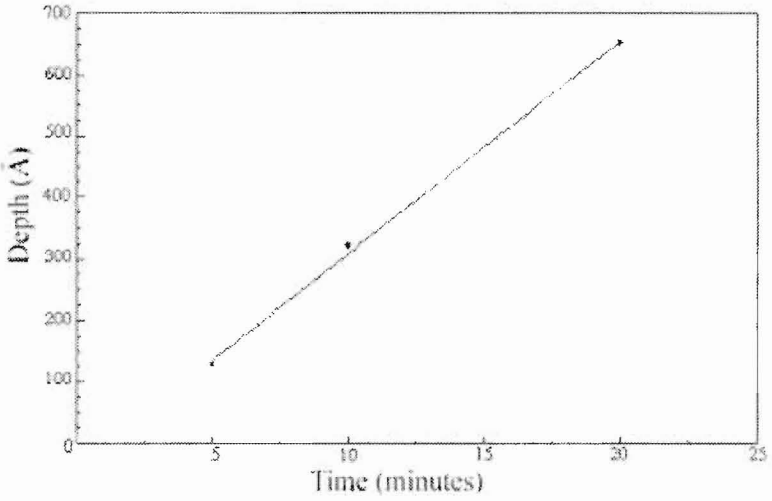

Figure 8: RIE of fused silica resulted in an etch rate of about 30 Å per minute. However, there may have been some additional etching due to physical bombardment.

IV. Analysis of the HOT Array

As we have seen, the laser power capable of reaching the focal plane is crucial for successful trapping. Although our holograms are designed to maximize power transmission, the basic concept of a HOT array necessarily distributes the power in some controlled way to each trap. It is necessarily, then, to carefully consider a HOT array in order to make sure its application is still reasonable and useful and an enormous amount of laser power is not needed to configure a large number of particles.

A. Trapping in Colloidal Solutions

In colloidal solution, the particles we trap will also be subjected to Brownian motion. So, we should compare our calculated trapping potential to $k_B T$ in order to determine whether the depth of the potential well formed by our optical tweezers is sufficient to hold the particle against thermal energies. This is done in Fig. 3 as the vertical axis is a dimensionless ratio of the reduced potential and thermal energy.

As we have seen, the reduction in electromagnetic potential energy is not significant when an ultra-small particle moves into the beam. From Fig. 3, we estimate that 1 mW is not sufficient to fix the positions of colloidal particles smaller than around 75 nm; below that size, Brownian motion will quickly remove particles from the trap. Moreover, if the medium is heated significantly, for example by absorption of either the trapping radiation or the illumination used for visualization, then this lower-limit on the trappable particle size would be correspondingly higher.

For a 1 μm silica particle (0.5 μm radius) immersed in water, and 1 mW of laser power transmitted through our specified optics, we find that the depth of the potential

well created by the trapping illumination is almost 250 times larger than k_BT. So, it would seem that such a particle ought to be very well trapped indeed, *if* the source used is capable of supplying 1 mW to the trap. However, if we were to reduce the amount of power devoted to this trap to 0.01 mW, the lifetime of the trapped configuration would be significantly shortened (the potential well would then be only 2.5 times k_BT). That is, the depth of the trapping potential is linearly dependent upon the available power.

We can roughly estimate the lifetime of the trapped configuration via a calculation that implicitly treats the optical potential as if it were a square well:

$$\frac{1}{\tau_{escape}} = \frac{1}{\tau_{attempt}} e^{-\frac{U}{k_B T}}, \text{ where } \tau_{attempt} = \frac{(well\ width)^2}{2D} \tag{12}$$

Taking the self-diffusion coefficient, D, of a silica particle in water[18] to be 0.4 $\mu m^2/s$ and assuming 1 mW per trap, we calculate the lifetimes shown in Fig. 9. Note that susceptibility to Brownian motion is reduced as the particle size increases. For example, if an experiment requires lifetimes on the order of 100 seconds, 1 mW would not be sufficient for any silica particle smaller than around 60 nm in radius, but the lifetime increases rapidly for larger particles. Obviously, the viscosity of the surrounding medium can also be chosen so as to minimize Brownian motion.

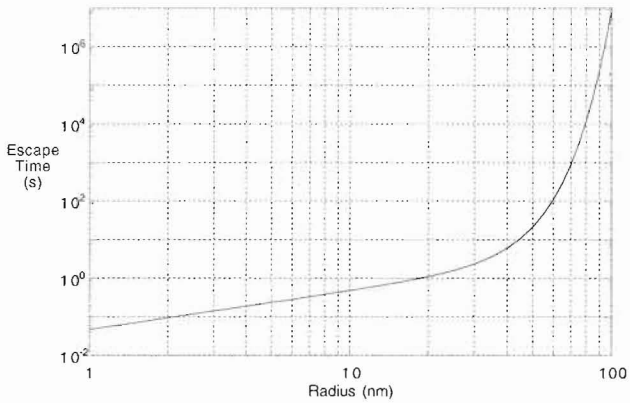

Figure 9: Given 1 mW of laser radiation and our optics, the lifetime of a silica particle trapped in water exceeds a day if its radius is larger than around 80 nm.

B. Factors Affecting the Number of Simultaneous Traps

For a tweezer setup using a single, discrete objective lens the field of view (FOV) may play some role in limiting the possible number of simultaneous optical traps. Assuming sufficient laser power is available, the maximum number of simultaneous optical traps would be achieved by a close-packed array. Yet, while an isolated trap can—in principle—localize a particle to a region much smaller than the resolution limit of the microscope, the modulation in the optical potential from well to well will vanish as the spacing between traps approaches the resolution limit of the optics. If the minimum allowable spacing between optical traps is $\beta\omega_0$ (where β is a factor of order unity), then the maximum number of simultaneously active optical traps is $2FOV/\left(\sqrt{3}(\beta\omega_0)^2\right)$. However, our current optics provide a FOV approximately 140 μm across; if $\beta \sim 5$, then the FOV would (for a maximally packed array) allow approximately 46,000 simultaneously active optical traps. Larger FOV is easily available, but taking 50,000 traps as an initial goal we might further examine the likely requirements.

In extending our earlier considerations to a design incorporating many traps, consider—initially—a HOT array that has been designed so as to distribute the laser power equally between all of the desired traps. We have already presented an intuitive, approximate calculation of the potential well depth for a single, well-isolated trap. It may then seem trivial to estimate the number of particles which can be simultaneously trapped, for a given laser power, particle size, material, surrounding medium, and angular divergence. For an optical setup like ours, we might require 0.1 mW per isolated trap; so, for example, in order to optically assemble a structure containing 50,000 particles, 5 Watts of laser power would seem necessary.

However, for HOT arrays, such calculations should only be taken as a guide; the laser power required to trap an isolated particle may be significantly different from the power required per trap in a large array. Particle-particle interactions and many-body effects may significantly raise or, in many cases, lower the power requirements. Notably, these additional optical and/or non-optical interactions may also allow the creation of arrays with a lattice constant much smaller than the minimum allowable spacing between *optical* traps, thereby increasing the number of configurable particles per FOV and reducing the power requirements of HOT arrays.

In addition to the incident light, *scattered* light from each trapped particle can induce dipole moments in neighboring particles. In essence, this is like a van der Waals interaction, except that it has been induced by an optical field and is, therefore, called optical binding (or Golovchenko binding, after its discoverer[41]). This coherent interaction of the dipole-dipole scattering between two trapped particles becomes significant as the

power devoted to the optical field becomes large. Nevertheless, in *many-body* HOT arrays, Golovchenko binding might play an important and useful role.

If the particles to be trapped are charged, coulombic interactions will clearly influence the potential landscape[22, 42-44] and can lead to pattern formation. Yet even for particles which are uncharged and nominally non-interacting, once entrained in a fluid each particle's motion can influence other, nearby particles. That is, medium-mediated interactions arise in the form of hydrodynamic coupling[15-16, 45] (*e.g.*, Bernouli effects) and/or entropic "coupling"[46] (if smaller particles are also present). Such interactions can add significant complexity to the stability of a HOT array.

In any cases where tweezing is primarily used to direct self-assembly of stable or metastable aggregations, power requirements may be minimal. Moreover, it may not be necessary that the laser power be distributed equally among all traps in a HOT array. Indeed those particles located in the interior of the array can typically be expected to require significantly less tweezing than their counterparts at the periphery. Holograms intended to take advantage of interactions between trapped particles could be designed so as to shunt the majority of the laser power to the most critical traps.

Clearly, then, there is no unique answer as to how many particles may be simultaneously trapped, or how small those particles may be. Particles which are well-trapped in vacuum might quickly escape if subjected to the buffeting associated with colloidal environments. The details of each experiment must be considered explicitly.

C. Hologram Fabrication Considerations

Ultimately, the number of simultaneous optical traps that is achievable may be limited by the challenges of patterning the necessary hologram. Roughly speaking, the minimum feature size needed in the hologram is $\delta x \sim f\lambda/L$, where f is the focal length, and L is the extent of the array. In our experiments, L is set by the FOV, which means—for our apparatus—the minimum feature size required in our holograms is $\delta x >$ 5 μm.

However, additional micro-optics might be fabricated so as to replace the microscope objective lens. This sort of apparatus is not limited by a FOV, so we might use a linewidth as small as $\delta x \sim \lambda/20$. In that case, the extent, L, of the trapping array could be no larger than about 20 times the focal length. Were such an "ultimate" array to contain traps spaced by $\beta\omega_0$, the maximum number of simultaneous active optical traps would be roughly $2\pi L^2 / \left(\sqrt{3}(\beta\omega_0)^2\right)$. For a micro-optic apparatus that matched our experimental parameters, this yields $\sim 10^{10}$ traps. While laser power and lithographic requirements of such a hologram would be daunting (a surface relief composed of 200 Å features spanning a couple of millimeters), the potential of HOT technology is clearly promising.

V. The HOT Apparatus

Schematically, the HOT apparatus is depicted in Fig. 10, where a laser beam incident on the holographic optic is diffracted and focused by a lens (the microscope objective in our setup). The resulting interference pattern is seen as an array of spots in the focal plane. There are several useful tools that can be incorporated into this basic HOT setup, which can aid in both the assembly and study of micro-particle arrays. One feature is dynamic, three-dimensional translation of the entire trapping array. This type of steering can be accomplished by adding a gimbal-mounted mirror into the optical path. This mirror can translate the beam along three dimensions and should be placed at a focal point. However, it is necessary that the back aperture of the objective remain at the final focal point—before the optical trap—so a telescope with magnification of one should be placed in between the steering mirror and the back aperture. A zooming lens may also be incorporated to expand the tweezer array while it is being focused. Similar considerations must be applied here where the optical design must make certain that the back aperture of the objective is always at the focal point. The zoom lens, along with the three-dimensional translation, might be used to shorten the time to fill each trap as these extra degrees of freedom lessen the limitation of having to wait for a particle to wander near a trap in order to be influenced by the potential well; the HOT can go directly to the particle and trap it. If the trap is strong enough, the array can continue to be slowly translated without the particles falling out due to resistance from the medium. The zoom lens might also be utilized to change the lattice spacing of the configured particles to aid, for example, in the analysis of two-dimensional colloidal crystals.

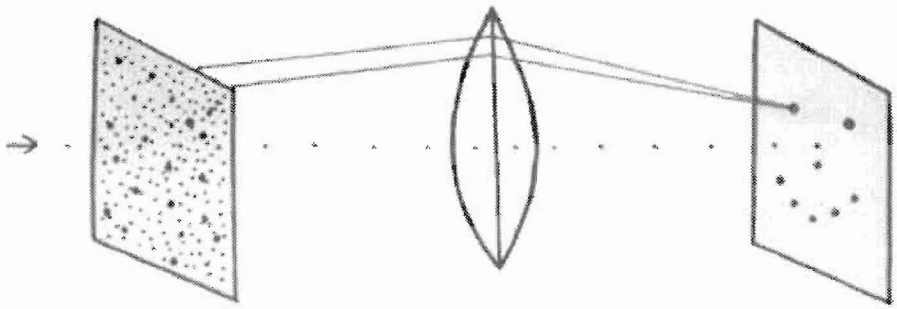

Figure 10: A simplified schematic of our HOT apparatus. A laser beam is incident on the hologram (left) and the diffracted rays are focused with a microscope objective lens (center). The final interference pattern appears at the focal plane where trapping occurs at each spot.

These useful tools, of course, require additional power-absorbing optics and can cause multiple reflections. Since our equations developed here involve the power of the laser beam after it has passed through all intervening optical elements, these trade-offs with additional optics must be taken into account when determining what initial laser power is needed. For example, a dichroic mirror is commonly placed in the optical path directly before the objective lens enabling a CCD camera to image through the objective while still being able to focus the laser beam. As this type of mirror will not be perfect, it allows some of the laser beam to be reflected and absorbed. To compare with our calculations, then, power levels should be measured at the point in the optical path where the particle is to be trapped (*i.e.*, the microscope's focal point). At the same time, assuming all intervening optics are of good quality and well-aligned, they should only absorb and reflect no more than a few percent of the total intensity. Anti-reflective coatings might even be considered not only for the optics, but for the incident side of the hologram as well to reduce intensity loss.

Optimization of the trapping potential is not merely a matter of power, but clearly depends upon power distribution. In order to maximize the transverse gradient,

significant laser power should be present at the furthest lateral extent of the objective lens. A simple telescope incorporated into the optical path (say, directly after the hologram) can expand the beam to match the diameter of the back aperture. It should be noted that, as the beam diameter is expanded, the tail of the Gaussian distribution is cut off, either by vignetting or by TIR. Thus there is a tradeoff between maximum power transmission and maximum transverse gradient. For optimization purposes, it may be useful to image the actual distribution of the beam intensity at the back aperture using photographic film or a CCD camera.

VI. Applications of HOT Arrays

Our first holograms have produced 4 × 4 arrays and hexagonal structures composed of 19, 0.5 μm radius silica particles (Fig 6). We will continue to produce larger arrays of assembled particles to fabricate interesting 2-D colloidal crystals. Once the crystal is formed, the laser will be blocked, and the melting of the crystal will be recorded by video microscopy with computer algorithms identifying and tracking each particle's position and velocity.[47]

As the hologram calculation and fabrication process is now well established, we will be capable of studying many types of crystal structures. We will construct a variety of 2-D particle configurations including various crystalline symmetries and quasicrystals, in each case specifying a range of surface terminations. We can incorporate dislocations, defect structures or form tailored potentials into the HOT array and see how they affect the integrity of the crystal. This degree of control will allow us to explore and create *models* of surface melting and related many-body effects. The physical mechanisms at the microscopic interface of two phases remains largely unknown. The utilization of holographic optical arrays will allow this study to have more control as researchers delve deeper into this uncharted territory.

Along with providing a practical means to study fundamental physics, holographically ordered colloidal crystals will make possible the fabrication of composite materials at the micron scale. By packing optical traps together with spacings less than a micron over the FOV of our microscope, we can use these colloidal crystals as masks for nano-sphere lithography (NSL). In addition, optical circuit elements and other extended structures and devices might be made by combining gelled arrangements of

microparticles.[18] Three-dimensionally ordered colloidal crystals can be used as chemical sensors and photonic circuit elements. Photonic bandgap materials (like optical waveguides) might be realized with the use of multilayer holographic tweezer arrays. Biological cells, for instance neurons, might be patterned into desired configurations to study how they grow, interconnect and interact.

Now that holographic images can be given real substance with our HOTs, we might see the first possibilities to developing imaging systems similar to the Star Trek Holodeck. Certainly, this application is a long way from being fully realized, but the essential features are in place: a computer calculation can convert any digital image into a hologram, through which a laser beam can pass and optically confine matter into a programmed position; virtual reality can now be made real. Additional fabricated micro-optics can replace the standard microscope optics that limit the extent to which HOT arrays can form. An entire room might be illuminated with a large number of HOTs as an intense spray of atoms engulfs the room until each trap is filled. When the user opens the door the recently fabricated world is complete. Dynamic holograms can make the real images move and interact with the user until the "End program" command is given where all the HOTs turn off and the real world disappears.

VII. Conclusion

Clearly, the addition of holographic techniques significantly extends the capabilities of laser tweezing, allowing for the simultaneous manipulation of large numbers of nanoparticles in a highly controllable way. While HOT assembly of functional structures should work with aerosols, in air, or in vacuum, as far as we know the method we have described is the *only* means of *fully* configuring an assembly of particles in solution. As the first to imbue computer-generated holograms with substance, we have produced the first complete implementation of a Holodeck: a laser beam which is passed through our computer-generated holograms forms a tailored array of "tractor beams" which causes nanoparticles to assemble themselves into the desired form. Given sufficient laser power, and a large effective FOV, extremely large numbers of particles may be programmed into position. Applications are envisioned in biology, chemistry, nanoelectronics, and the production of photonically-active materials.

Acknowledgements

I would like to thank Dr. H. P. Goeckner for suggestions made with the potential calculations, E. R. Dufresne for his introduction to optical tweezers and D. G. Grier for support and guidance. Especially, I owe a great deal of gratidute to my advisor, Dr. G. C. Spalding, who has brought me extraordinary research opportunities. His love and drive to help me learn cool physics and succeed in my work has firmly set me on an exciting path to becoming a successful experimental physicist. Thanks Gabe.

In addition, I would like to thank the support from the Council on Undergraduate Research, the National Science Foundation Research Experience for Undergraduates, the Illinois Wesleyan University βββ Research Grant, the Illinois Wesleyan University Anderson Physics Scholarship, and the Barry M. Goldwater Fellowship.

References

1. S. P. Smith, S. R. Bhalotra, A. L. Brody, B. L. Brown, E. K. Boyda, and M. Prentiss, Am. J. Phys. **67**, 26-35 (1999).

2. M. T. Dearing, G. C. Spalding, in *Materials Issues and Modeling for Device Nanofabrication*, edited by L. Merhari, L. T. Wille, K. Gonsalves, M. F. Gyure, S. Matsui, L. J. Whitman (Mater. Res. Soc. Proc., Boston, MA, 2000).

3. A. Ashkin, J. M. Dziedzic, J. E. Bjorkholm, S. Chu, *Opt. Lett.* **11**, 288-290 (1986).

4. A. Ashkin, *Bio. Journ.* **61**, 569-582 (1992).

5. Y. Harada, T. Asakura, *Optics Comm.* **124**, 529-541 (1996).

6. T. N. Buican, M. J. Smyth, H. A. Crissman, G.C. Salzman, C. C. Stewart, J. C. Martin, *App. Opt.* **26**, 5311-5316 (1987).

7. A. Ashkin, J. M. Dziedzic, T. Yamane, *Nature* **330**, 769-771 (1987).

8. A. Ashkin, J. M. Dziedzic, *Science* **235**, 1517-1520 (1987).

9. S. M. Block, D. F. Blair, H. C. Berg, *Nature* **338**, 514-518 (1989).

10. M. W. Berns, W. H. Wright, B. J. Tromberg, G. A. Profeta, J. J. Andrews, R. J. Walter, *Proc. Natl. Acad. Sci. USA*, **86**, 4539-4543 (1989).

11. S. Sato, Y. Harada, Y. Waseda, *Opt. Lett.*, **19**, 1807-1809 (1994).

12. S. Chu, J. E. Bjorkholm, A. Ashkin, A. Cable, *Phys. Rev. Lett.*, **57**, 314-317 (1986).

13. K. Visscher, S. P. Gross, S. M. Block, *IEEE J. Selected Topics in Quantum Electronics* **2**, 1066-1076 (1996).

14. E. Fällman, O. Axner, *App. Opt.* **36**, (1997).

15. J. C. Crocker, *J. Chem. Phys.*, **106**, 2837-2840 (1997).

16. J. Meiners, S. R. Quake, *Phys. Rev. Lett.*, **82**, 2211-2214 (1999).

17. J. C. Crocker, J. A. Matteo, A. D. Dinsmore, A. G. Yodh, *Phys. Rev. Lett.* **82**, 4352 (1999).

18. E. R. Dufresne, D. G. Grier, *Rev. Sci. Instr.* **69**, 1974-1977 (1998).

19. E. Lidorikis, Q. Li, C. M. Soukoulis, *Phys. Rev. E* **55**, 3613-3618 (1997).

20. V. Yannopapas, N. Stefanou, A. Modinos, *J. Phys.: Condens. Matt.* **9**, 10261-10270 (1997).

21. A. Imhof, W. L. Vos, R. Sprik, A. Lagendijk, *Phys. Rev. Lett.*, **83**, 2942-2945 (1999).

22. J. C. Crocker, D. G. Grier, *Phys. Rev. Lett.* 73, 352-355 (1994).

23. R. Geer, T. Stoebe, C. C. Huang, R. Pindak, J. W. Goodby, M. Cheng, J. T. Ho, S. W. Hui, *Nature* **355**, 152-154 (1992).

24. J. C. Zahorchak, R. Kesavamoorthy, R. D. Coalson, S. A. Asher, *J. Chem. Phys.* **96**, 6873-6879 (1992).

25. K. J. Naidoo, J. Schnitker, *J. Chem. Phys.* **100**, 3114-3121 (1994).

26. J. Chakrabarti, H. R. Krishnamurthy, A. K. Sood, *Phys. Rev. Lett.* **73**, 2923-2926 (1994).

27. J. Chakrabarti, H. R. Krishnamurthy, A. K. Sood, S. Sengupta, *Phys. Rev. Lett.* **75**, 2232-2235 (1995).

28. A. E. Larsen, D G. Grier, *Phys. Rev. Lett.* **76**, 3862 (1996).

29. D. G. Grier, *Nature* **379**, 773 (1996).

30. M. R. Sadr-Lahijany, P. Ray, H. E. Stanley, *Phys. Rev. Lett.* **79**, 3206-3209 (1997).

31. J. A. Weiss, A. E. Larsen, D. G. Grier, *J. Chem. Phys.* **109**, 8659 (1998).

32. E. Frey, D. R. Nelson, L. Radzihovsky, *Phys. Rev. Lett.* **83**, 2977-2980 (1999).

33. *e.g.*, B. E. A Solah, M. C Teich, *Fundamentals of Photonics* (Wiley, New York, 1991).

34. J. P. Barton, D. R. Alexander, *J. Appl. Phys.* **66**, 2800-2802 (1989).

35. T. Tlusty, A. Meller, R. Bar-Ziv, *Phys. Rev. Lett.* **81**, 1738-1741 (1998).

36. S. G. Lipson, H. Lipson, and D. S. Tannhauser. *Optical Physics, 3rd Ed.* (Cambridge University Press, Cambridge, 1995).

37. V. Soifer, V. Kotlyar, and L. Doskolovich, *Iterative Methods for Diffractive Optical Elements Computation* (Taylor & Francis, London, 1997).

38. J. Sanny, W. Moebs, *University Physics* (Wm. C. Brown, Dubuque, IA, 1996).

39. G. J. Swanson, W. B. Veldkamp, *Optical Engineering* **28**, 605-608 (1989).

40. H. P. Herzig, Ed., *Mico-Optics: Elements, systems and applications* (Taylor & Francis, Bristol, PA, 1997).

41. M. W. Burns, J. Fournier, and J. A. Golovchenko, *Science* **249**, 749-754 (1990).

42. R. van Roij, J. Hansen, *Phys. Rev. Lett.* **79**, 3082-3085 (1997).

43. G. C. de León, J. M. Saucedo-Solorio, J. L. Arauz-Lara, *Phys. Rev. Lett.* **81**, 1122-1125 (1998).

44. E. Allahyarov, I. D' Amico, H. Löwen, *Phys. Rev. Lett.* **81**, 1334-1337 (1998).

45. E. R. Dufresne, T. M. Squires, M. P. Brenner, D. G. Grier, *Phys. Rev. Lett.* (submitted).

46. R. Verman, J. C. Crocker, T. C. Lubensky, A. G. Yodh, *Phys. Rev. Lett.* **81**, 4004-4007 (1998).

47. J. C. Crocker, D. G. Grier, *J. Colloid Interface Sci.* **179**, 298-310 (1996).